Nonvolatile and Volatile Skyrmion Generation Engineered by Ionic Liquid Gating in Ultrathin Films

Yao Zhang[1,2,3] Guy Dubuis,[1,2,4] Colin Doyle[5] Tane Butler,[1,2,3] and Simon Granville[1,2,*]

[1] *Robinson Research Institute, Victoria University of Wellington, Wellington 6140, New Zealand*
[2] *MacDiarmid Institute for Advanced Materials and Nanotechnology, Wellington 6012, New Zealand*
[3] *School of Chemical and Physical Sciences, Victoria University of Wellington, Wellington 6140, New Zealand*
[4] *Measurement Standards Laboratory, 69 Gracefield Road, Lower Hutt 5010, New Zealand*
[5] *Department of Chemical and Materials Engineering, The University of Auckland, Private Bag 92019, Auckland 1042, New Zealand*

Magnetic skyrmions are topological spin textures with nanoscale size, which have great potential for spintronics applications. However, they are very sensitive to film thicknesses and interfaces in ultrathin films or multilayer heterostructures, and methods to generate and tune skyrmions are needed in order to use them in real-world applications. Electric field gating has been shown to modify the magnetic characteristics of thin films; however, these changes are limited by the low electric fields achievable using solid gate electrodes. In this work, we use ionic liquid gating to modify the magnetic characteristics of perpendicularly magnetized $MgO/Mn_2CoAl/Pd$ ultrathin films, applying a range of voltage sequences to generate skyrmions through both nonvolatile and volatile changes to these films. We achieve a giant anisotropy field tunability of 109.8 mT V^{-1} that is nonreversible, which can be ascribed to magneto-ionic effects. Reversible changes to the anisotropy and volatile skyrmion formation are achieved via electrostatic charge accumulation, which could induce an in-plane Rashba field. Our results strongly demonstrate that ionic liquid gating is a versatile method to engineer both nonvolatile and volatile skyrmions by tuning the magnetic characteristics of films to the regimes where they can exist.

I. INTRODUCTION

Topologically nontrivial states have attracted great interest in condensed-matter physics due to the emergent phenomena and potential applications [1]. Magnetic skyrmions are topologically protected whirling spin textures with nanoscale dimension, which can be used as information carriers and have great potential applications for magnetic memory, logic gates, and computing [2,3]. They have been observed in single crystals with a noncentrosymmetric lattice [4] and in ultrathin films or multilayer heterostructures [5–7]. For ferromagnet–heavy-metal ultrathin-film bilayers or multilayers with perpendicular magnetic anisotropy (PMA), skyrmions can be stabilized by the competition of interactions among the exchange interaction, the magnetic anisotropy, and the Dzyaloshinskii-Moriya interaction (DMI) [8]. The DMI is a chiral interaction originating from strong spin-orbit coupling and inversion symmetry breaking at the interface between the ferromagnetic and heavy-metal layers that can induce a noncollinear spin texture [9,10]. By tuning

these interactions, one can obtain various magnetic ground states, such as uniform ferromagnetic domains, labyrinth domains, and skyrmions [6,11].

Recently, by varying the thickness of the ferromagnetic layer, Soumyanarayanan *et al.* have tailored both the effective magnetic anisotropy and the DMI and thus observed skyrmions with different sizes and densities [7]. Hervé *et al.* have found that isolated skyrmions can be stabilized in a monolayer of Co/Ru(0001) with weak spin-orbit coupling due to the absence of magnetic anisotropy energy [12]. Skyrmions can also be observed near the spin-reorientation transition by inserting an Os layer at the interface of Co and Pt, due to the reduction of the saturation magnetization and the effective magnetic anisotropy [13]. However, in those works, skyrmions only appear in a very narrow range of thicknesses where the PMA is weak, so it can require an extensive experimental campaign to produce multiple samples in attempts to find that narrow range. This is a challenge for sample preparation and is curtailing possible applications. Recent attempts to speed up the development of optimized skyrmion structures include a combinatorial-like method of depositing double-wedged samples with a continuously varying anisotropy and DMI [14]. To truly

---

*simon.granville@vuw.ac.nz

014030-1

speed up the work to optimize skyrmion conditions, it would be most useful to develop a method to adjust the relevant magnetic parameters that produce skyrmions after a sample has been produced.

One such method to engineer the magnetic anisotropy and DMI in thin films is electric field gating. Recently, the generation of skyrmions by this method has been demonstrated in various systems with PMA, such as Pt/Co/oxide [15], Ta/Co-Fe-B/TaO$_x$ [16], Ir-Mn/Co-Fe-B/MgO [17], and Pt/Co-Ni multilayers [18], due to the rise of the DMI or reduction of the PMA. However, these works employ a conventional field-effect transistor (FET) -like structure using thick insulating gate dielectrics, such as SiO$_2$ or HfO$_2$, with relatively small charge carrier densities resulting in a small capacitance and electric field [19]. Inevitably, skyrmions have only been generated in thin films with a magnetic anisotropy closing to the spin-reorientation transition between the out-of-plane (OP) and in-plane (IP) directions at a large gate voltage. Instead of using a solid-state dielectric, ionic liquid gating (ILG) using ionic liquids or ion gels has been demonstrated as a powerful method to effectively tune the magnetic anisotropy in thin films [20,21] and the DMI [22]. This method is also referred to as electric double-layer gating (EDLG). Using this method, an ultrahigh electric field can be generated at the electric double-layer interface over a nanometer-scale gap between the ions in the Helmholtz layer and the charge carriers in the sample [23]. This interfacial gating behavior can lead to controlled and reversible changes of carrier concentration and to a magneto-ionic effect [19]. It can thus achieve substantial modifications of magnetic anisotropy and the DMI. Recently, using ILG, a high-voltage-controlled magnetic anisotropy coefficient of 14.6 mT V^{-1} [21] and approximately 0.5 mJ m^{-2} DMI modification [22] have been achieved. Thus, ILG can be a useful method to engineer magnetic interactions as mentioned above and generate skyrmions at a low gate voltage.

In this work, we investigate MgO/Mn$_2$CoAl/Pd ultrathin films with PMA by ILG. We demonstrate that ILG can generate both nonvolatile and volatile skyrmions. Nonvolatile skyrmions can be generated at a negative gate voltage in ultrathin films starting with either weak or intermediate PMA due to a magneto-ionic effect. What is more, volatile skyrmions can be generated at a small positive gate voltage after applying a large trigger gate voltage, which can be explained by electrostatic charge accumulation. All skyrmion-generation modes happen at thicknesses slightly outside the range where skyrmions appear in pristine samples, demonstrating that ILG is a versatile technique to fine tune the magnetic anisotropy and DMI strength so that the magnetic texture can be designed and optimized without the need for combinatorial growth of thin films to achieve precisely varied magnetic parameters in as-grown samples.

II. EXPERIMENTAL METHOD

Ultrathin films consisting of MgO/Mn$_2$CoAl/Pd trilayers are deposited on thermally oxidized Si substrates by magnetron sputtering with a base pressure below 4×10^{-8} Torr. Samples are grown at ambient temperature while rotating the sample holder and then postannealed *in situ* for 1 h at 300°C. MgO is rf sputtered with 100-W and 3-mTorr Ar at a growth rate of 0.05 Å/s. Mn$_2$CoAl and Pd are dc sputtered with 100-W 5-mTorr Ar and 20-W 2-mTorr Ar, respectively, at a growth rate of 0.84 and 0.46 Å/s, respectively. For more information about the sample fabrication, see our previous work [24,25].

A small droplet of ionic liquid, *N*,*N*-diethyl-*N*-methyl-*N*-(2-methoxyethyl)ammonium bis(trifluoromethylsulfonyl)imide (DEME TFSI) (IoLiTec), is used as the electrolyte connecting the Pt gate electrode and the surface of sample, as shown in Fig. 1(a). In order to obtain a uniform thickness, a piece of glass cover slide (100 μm thick) is placed on the ionic liquid. This ensures an aberration-free optical path for the magneto-optical Kerr effect (MOKE) measurement. The charging process is as follows: (i) for the weak-PMA sample [MgO(1.6 nm)/Mn$_2$CoAl(2.6 nm)/Pd(3.2 nm)], as shown in Fig. 1, the charging route is 0 V → 1.5 V → 0 V → −2.5 V with a step of 0.5 V; (ii) for the intermediate-PMA sample [MgO(1.6 nm)/Mn$_2$CoAl(2.6 nm)/Pd(2.8 nm)] under the cycling charging method, as shown in Fig. 3, the charging route is 0 V → [−2.5 V → 1 V]$_{n=31}$ → −2.5 V → 0 V (where *n* corresponds to the number of cycles); (iii) for the weak-PMA sample [MgO(1.6 nm)/Mn$_2$CoAl(2.6 nm)/Pd(3.2 nm)] under the trigger charging method, as shown in Fig. 4, the charging route is 0 V → −3 V(charge 2 min)→ −0.5 V → [1.5 V → 0 V]$_{n=10}$, or 0 V → −3 V(charge 2 min)→ 0 V → 1.7 V → 0 V. All samples are charged for 5 min at each gate voltage except for the trigger voltage −3 V.

Unless indicated otherwise, samples are charged for 5 min at each voltage to reach the equilibrium of carriers. The gate voltage is applied by a Keithley 2450 source meter. These gating experiments are carried out in ambient atmosphere at room temperature.

Magnetization measurements are performed using the reciprocating-sample-option (RSO) module of a superconducting-quantum-interference-device (SQUID) magnetometer (MPMS-XL, Quantum Design) and MOKE measurements with a green light ($\lambda = 540$ nm) are used to image the magnetic domain morphology, using a MagVision Kerr microscopy system in differential imaging mode with a $50\times$ magnification objective having a numerical aperture of 0.6 and a spatial resolution of 50 nm per pixel. The samples are first charged under a gate voltage for 5 min without a magnetic field and then the hysteresis loops and domain images are simultaneously taken by sweeping
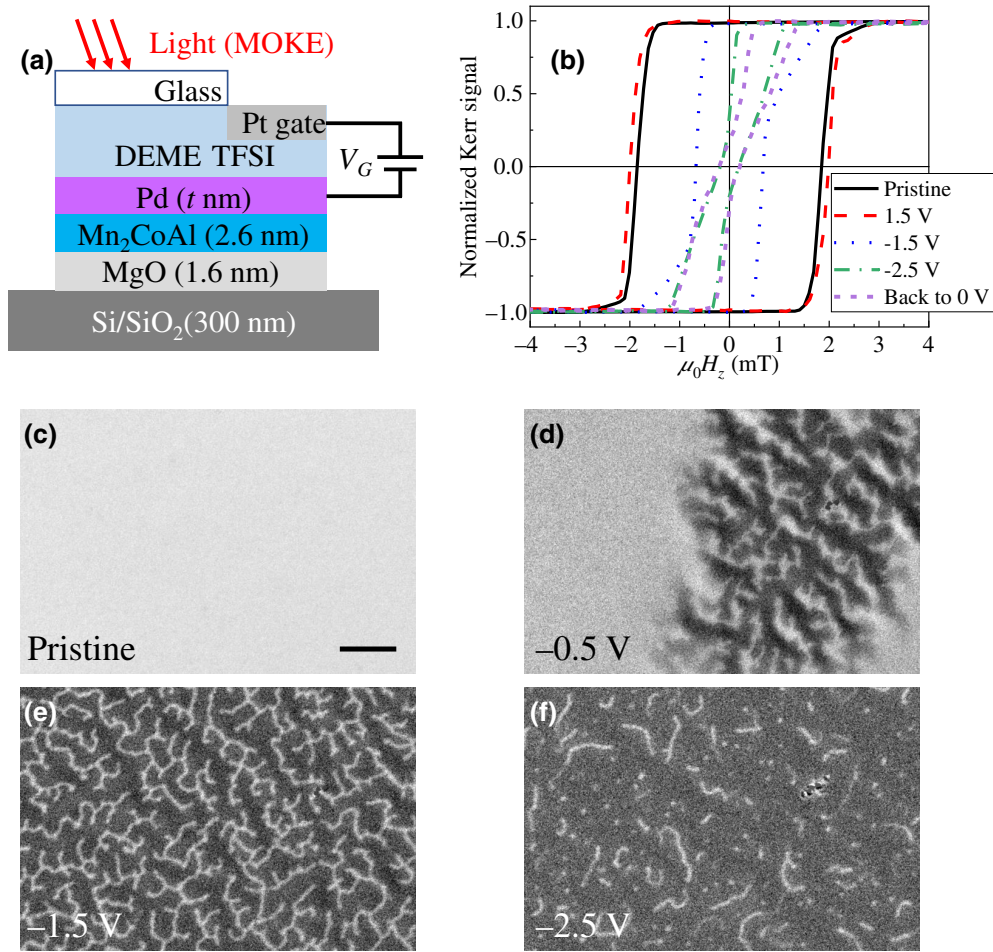
FIG. 1. A schematic of the device and the gate-dependent magnetic characterization. (a) A schematic of the ionic liquid device for MgO/Mn$_2$CoAl/Pd stacks. (b) The gate dependence of hysteresis loops measured in an OP magnetic field at ambient temperature for MgO(1.6 nm)/Mn$_2$CoAl(2.6 nm)/Pd(3.2 nm) stack. (c)–(f) The corresponding magnetic domain images, captured under $\mu_0 H_z = 1.0$ mT in the pristine state and at -0.5, -1.5, and -2.5 V, respectively. The scale bar in (c) corresponds to 10 μm.

the magnetic field from positive to negative in an interval of 0.1 mT under the gate voltage (this measurement takes less than 2 min), i.e., the domain images are captured at each magnetic field step.

X-ray photoelectron spectroscopy (XPS) measurements are carried out using a Kratos Axis UltraDLD system (Kratos Analytical Ltd., Wharfside, Manchester, UK). The measurements are made using a monochromatic Al K$_\alpha$ x-ray source. Prior to measurement, the gated samples are rinsed with ethanol and deionized water to remove the ionic liquid residual, followed by a gas blow dry, and then transferred into the XPS chamber. For the depth-profile measurement, a 5-kV Ar$^+$ beam is rastered over a 3×3 mm area with data collected from a 110×110 μm location centered within the etch area. The Kratos Mini Beam III ion gun is run with an 8-mA emission current and a 5-kV accelerating voltage. The peak fitting of the resultant spectra is carried out using CasaXPS.

III. RESULTS

A. Nonvolatile skyrmion generation by ionic liquid gating

The magnetic hysteresis loops for the MgO(1.6 nm)/Mn$_2$CoAl(2.6 nm)/Pd(3.2 nm) ultrathin film are measured by polar MOKE in a sweeping OP magnetic field at ambient temperature, as shown in Fig. 1. Figures 1(c)–1(f) show the corresponding magnetic domains under an OP field of -1 mT after sweeping from positive magnetic saturation field. This pristine sample shows clear PMA with a coercive field of $\mu_0 H_c = 1.85$ mT [Fig. 1(b)] and a uniform magnetization at -1 mT [Fig. 1(c)]. The anisotropy field $\mu_0 H_k$ is found to be 163 mT, fitted by the Stoner-Wohlfarth model (see Fig. S1 in the Supplemental Material [26]). Thus, the effective magnetic anisotropy constant $K_{\text{eff}} = (1/2)\mu_0 H_k M_s$ is 2.56×10^4 J m^{-3}, where $M_s = 3.15 \times 10^5$ A m^{-1} is the saturation magnetization

obtained from a SQUID measurement at 300 K. The DMI coefficient, D, is calculated by the method set out in our previous work [25]. For ultrathin films with PMA, given that the energy difference between the stripe and labyrinth domains is very small and when the thickness of the ferromagnetic layer, t, is much smaller than the domain width, the domain-wall energy of the labyrinth domains, σ_{DW}, can be written as [27]

$$\sigma_{DW} = \frac{\mu_0 M_s^2 t}{\pi} \ln \frac{d}{0.955t}, \tag{1}$$

where d is the width of the domain period. The value of d is extracted from the demagnetized domain image using a two-dimensional fast Fourier transform, as shown in Fig. S2 in the Supplemental Material [26]. Thus, one can obtain D by means of

$$\sigma_{DW} = 4\sqrt{A_{ex}K_{eff}} - \pi D, \tag{2}$$

where A_{ex} is the exchange stiffness. D can be calculated as 0.36 mJ m^{-2} with $t = 2.6$ nm, $d = 4500$ nm, and $A_{ex} = 8.99$ pJ m^{-1} [25] for the film in the pristine state. Under this magnitude of DMI, Néel-type chiral domain walls are expected, which have been confirmed by using the asymmetric domain-wall expansion method in this MgO/Mn$_2$CoAl/Pd trilayer system [25]. Then, we start to apply a gate voltage (V_G) on the stack. At $V_G = 1.5$ V, $\mu_0 H_c$ increases slightly to 2 mT and there is no change to the magnetic domains at -1 mT. By changing V_G to -0.5 V, the labyrinth domains start to nucleate from the uniform ferromagnetic state [see Fig. 1(d)]. At a negative $V_G = -1.5$ V, $\mu_0 H_c$ shrinks significantly, to 0.67 mT, and the magnetic moment transition is not sharp near the saturation regime. Furthermore, only labyrinth domains can be observed [see Fig. 1(e)]. By continuing to increase V_G to -2.5 V, $\mu_0 H_c$ shrinks to 0.18 mT and the remanent state is no longer saturated, indicating that the magnetic anisotropy approaches the spin-reorientation transition between the OP and IP directions. Interestingly, skyrmions with an average diameter of approximately 1 μm can be generated and can coexist with labyrinth domains, as shown in Fig. 1(f). After setting the voltage back to 0 V for 5 min, $\mu_0 H_c$ and the skyrmions stay at the same magnetic field as they are with $V_G = -2.5$ V, showing that this ILG effect is nonvolatile, which means that the magnetic behavior of the thin films can be retained once the voltage is switched off. This is in contrast to volatile behavior, which means that the magnetic state would revert to the initial state when the power is switched off.

Given that skyrmions originate from the competition between magnetic anisotropy and the DMI, we calculate K_{eff} and D at various gate voltages, as shown in Fig. 2. We suppose that M_s is constant under each gate voltage, since our XPS results show no changes to the ferromagnetic Mn$_2$CoAl layer after gating, as is discussed later. The
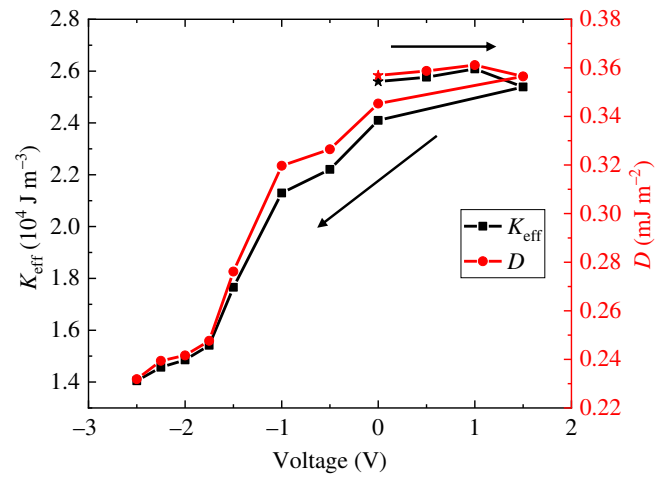

FIG. 2. The effective magnetic anisotropy, K_{eff}, and the DMI coefficient D as a function of the gate voltage for a MgO(1.6 nm)/Mn$_2$CoAl(2.6 nm)/Pd(3.2 nm) stack. The star and the arrows correspond to the pristine state and the charging process, respectively.

influence on K_{eff} is very small at a positive gate voltage. However, K_{eff} decreases significantly with an increasing negative gate voltage. In particular, at -2.5 V, K_{eff} drops to 1.4×10^4 J m^{-3} with a remarkable anisotropy field tunability of 29.3 mT V^{-1}, which is twice the previous record [21]. The change in trend of D as a function of the gate voltage is similar to that of K_{eff}. At $V_G = -2.5$ V, D decreases by 35% to 0.23 mJ m^{-2}. Usually, to obtain skyrmions in ultrathin films, samples should exhibit a weak K_{eff} or a comparatively large D [6,12]. Even though the value of D decreases at a negative voltage, the rate of the K_{eff} decrease is greater than that of D. What is more, a very small value of K_{eff} has been reached at -2.5 V, where the magnetic anisotropy closes to the spin-reorientation transition, in which skyrmions can be easily annihilated [13]. Previous research has shown that $D \sim 0.25$ mJ m^{-2} is enough to stabilize skyrmions in Ta/Co-Fe-B/MgO with $K_{eff} \sim 3.3 \times 10^4$ J m^{-3} [28,29]. By using ILG, we are able to reduce the PMA in our thin films to a very weak $K_{eff} = 1.4 \times 10^4$ J m^{-3} with $D = 0.23$ mJ m^{-2}, reaching the regime where skyrmions are stabilized by the DMI. The magnetic configuration of the skyrmions is expected to be of the right-handed Néel type, the same as that of the domain walls, as shown in our previous work [25].

B. Nonvolatile skyrmion generation in intermediate-PMA trilayers

For thin films with a small $\mu_0 H_c$ and a weak K_{eff}, a single gate voltage, less than -2.5 V, is enough to reduce the PMA into a region where skyrmions can be generated, as shown above. It should be noted that, in this work, thin films with a weak PMA are defined such that the magnetic anisotropy closes to the spin-reorientation transition

between the OP and IP directions. In the case of samples with an intermediate or strong K_{eff}, which usually show a large coercive field, one has to apply a large single voltage to create skyrmions. However, electrochemical reactions can happen at large voltages [30], which could significantly change the properties or even damage the sample. To generate skyrmions in a thin film with an as-grown intermediate PMA, we employ an alternative gating method by repeatedly cycling the gate voltage from -2.5 V to 1 V. We start with a MgO(1.6 nm)/Mn$_2$CoAl(2.6 nm)/Pd(2.8 nm) trilayer that has an intermediate-strength PMA with $K_{eff} = 5.76 \times 10^4$ J m^{-3} and $\mu_0 H_c = 8.46$ mT, as shown in Fig. 3(a). Due to these large magnetic parameters, we cannot obtain the periodic demagnetized domains and thus we cannot calculate the DMI using the method mentioned above. Figures 3(b)–3(d) and 3(f)–(h) show the magnetic hysteresis loops at -2.5 V after different numbers of cycles and the corresponding magnetic morphology at 0.66 mT, respectively. Essentially, $\mu_0 H_c$ decreases with repeated cycling, and finally tends toward saturation, which resembles the training effect of exchange bias in antiferromagnet-ferromagnet bilayers, in which the exchange bias field gradually degrades upon repeated magnetic field cycling [31]. For instance, after cycling 21 times, a square loop can still be observed but $\mu_0 H_c$ decreases significantly to 0.68 mT and labyrinth domains nucleate from the uniform ferromagnetic state, as shown in Figs. 3(b) and 3(f), respectively. For 27 cycles, the shape of the hysteresis loop looks similar to the green one in Fig. 1(b) after applying $V_G = -2.5$ V. Both of these exhibit similar magnetic morphology in which the coexistence of skyrmions and labyrinth domains can be observed [compare Fig. 3(g) to Fig. 1(f)]. After 30 cycles, K_{eff} decreases to 1.44×10^4 J m^{-3} with a giant anisotropy field tunability of 109.8 mT V^{-1} and only skyrmions can be observed, as shown in Fig. 3(h). Figure 3(i) shows the evolution of $\mu_0 H_c$ at -2.5 or 1 V by increasing cycles. Up to 20 cycles, the value of $\mu_0 H_c$ decreases at $V_G = -2.5$ V after each cycle and then recovers a little at $V_G = 1$ V, which is in line with the results of Fig. 1(b). Beyond 20 cycles, $\mu_0 H_c$ decreases slowly and tends toward saturation. Furthermore, the value of $\mu_0 H_c$ does not change by setting the voltage back to 0 V, demonstrating that this ILG behavior is nonvolatile. This gating method works for a weak-PMA sample as well. Here, we choose to show only the results for the intermediate-PMA sample with a larger $\mu_0 H_c$, because it is better to show the capacity for the gate-voltage-cycling generation of skyrmions starting from a stronger K_{eff}.

C. Volatile skyrmion generation by ionic liquid gating

It is also possible to use ILG to change the magnetic anisotropy and the coercive field and generate skyrmions in a volatile mode, i.e., the skyrmions disappear when the gate voltage is removed. We start with a MgO(1.6

nm)/Mn$_2$CoAl(2.6 nm)/Pd(3.2 nm) ultrathin film, which has an initial anisotropy close to the sample of Figs. 1–2, i.e., weak anisotropy. We first apply a large trigger voltage of $V_G = -3$ V for charging for 2 min and then we reduce V_G to -0.5 V. The square hysteresis loop indicates PMA, as shown in Fig. 4(a). Subsequently, a positive V_G = 1.5 V is applied. Interestingly, the square loop disappears, indicating that the PMA is entirely lost [see Fig. 4(b)]. To prove that the magnetic moments rotate to the IP direction rather than that the magnetization has been destroyed, the *in situ* longitudinal geometry of a MOKE measurement is performed by sweeping an IP magnetic field. Figure 4(c) shows the longitudinal Kerr signal of the gated thin film at 1.5 V. A clear loop can be observed, demonstrating that a switch of the anisotropy from the OP to the IP direction is achieved. When V_G is set back to -0.5 V, the PMA is spontaneously recovered with a loop that is indistinguishable from the first -0.5 V loop, as shown by the red curve in Fig. 4(a). Figure 4(d) presents the reversibility of $\mu_0 H_c$ and the ratio of the remnant magnetization (M_r) to M_s as V_G is cycled ten times between 1.5 and -0.5 V. Both $\mu_0 H_c$ and M_r/M_s can be reversibly and nondestructively toggled into the IP direction with a small positive voltage. What is more, skyrmions can be observed by using this charge method. Again, we apply a trigger -3 V and then revert to 0 V. The sample starts with PMA, as shown in Fig. 4(e). After that, a positive $V_G = 1.7$ V is applied and one obtains a hysteresis loop with a shape that looks similar to the green one in Fig. 1(b), which exhibits skyrmions. Figures 4(g) and 4(h) show the corresponding domain images under $\mu_0 H_z = 1.1$ mT, at 0 and 1.7 V, respectively. Labyrinth domains can be observed at 0 V and then skyrmions are created at 1.7 V. By setting V_G back to 0 V, the PMA is totally recovered, as shown by the red loop in Fig. 4(e), demonstrating that this ILG behavior is volatile. This triggering method works for the intermediate-PMA sample as well.

D. Surface analysis

It is well known that the ILG modification is related to electrostatic charging, the magneto-ionic effect, and the electrochemical reaction [19]. To understand the potential mechanisms in our study, XPS, a surface technique, is employed to characterize the oxidation or chemical-state information of our ultrathin films using different ILG methods, as shown in Fig. 5. Figures 5(a) and 5(b) show scans of the regions for Pd $3d$ and $3p_{3/2}$ core levels, respectively, and a corresponding peak fitting for the weak-PMA sample with a 3.2 nm Pd layer in the pristine state. The fits to the XPS results use the Pd $3d_{5/2}$ and $3p_{3/2}$ peaks that are centered at 335.0 and 531.4 eV, respectively [32]. The spectrum presented in Fig. 5(a) shows a spin-orbit split doublet consistent with metallic Pd, with the $3d_{5/2}$ and
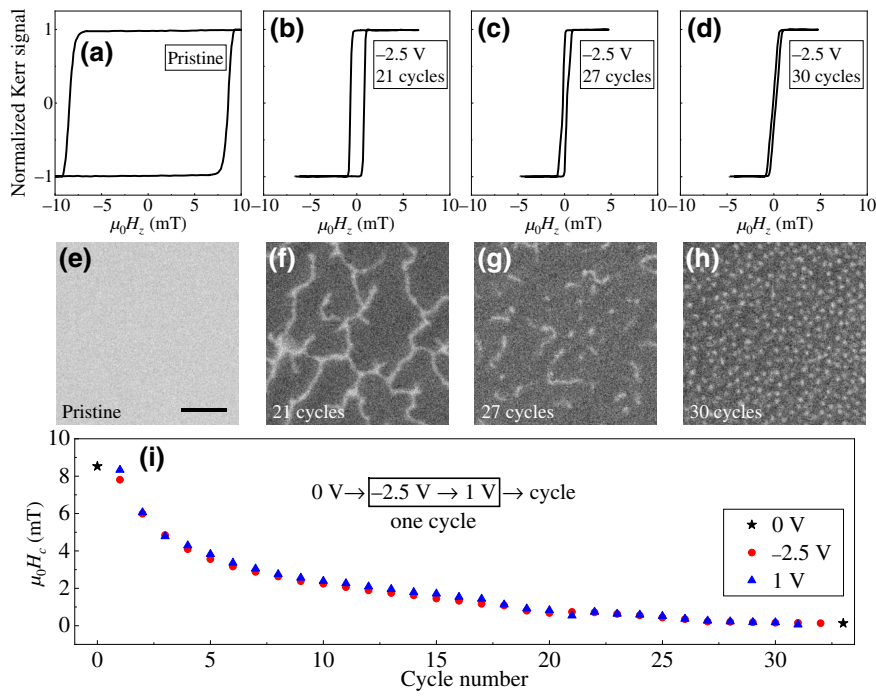
FIG. 3. The evolution of hysteresis loops and magnetic domains. (a) The hysteresis loop of a MgO(1.6 nm)/Mn$_2$CoAl(2.6 nm)/Pd(2.8 nm) trilayer in the pristine state. (b)–(d) Hysteresis loops at −2.5 V after cycling 21, 27, and 30 times, respectively. (e)–(h) The corresponding magnetic domain images, with $\mu_0 H_z = 0.66$ mT, captured from (a)–(d), respectively. The scale bar in (e) corresponds to 10 μm. (i) $\mu_0 H_c$ as a function of the cycle number for 1 and −2.5 V, respectively.

$3d_{3/2}$ appearing as well-separated peaks. At a higher binding energy, there is a second species present, with weak peaks at 341.5 and 336.3 eV, respectively, representing O—Pd bonds [33], which suggests that there is a very thin native-oxide PdO$_x$ layer. To confirm the oxidation of Pd, the O 1s spectrum is scanned, although it is very close to the $3p_{3/2}$ line in Fig. 5(b). One can observe a clear shoulder

at 529.0 eV on the low-binding-energy side of the Pd $3p_{3/2}$ peak, which is consistent with an O 1s peak, as shown in Fig. 5(b). It should be noted that there is no evidence that this O 1s peak could be derived from the MgO or SiO$_2$ layers, as no evidence for either Mg or Si is observed in the survey spectra. A simple consideration of the escape depth of an electron also precludes the oxygen observed
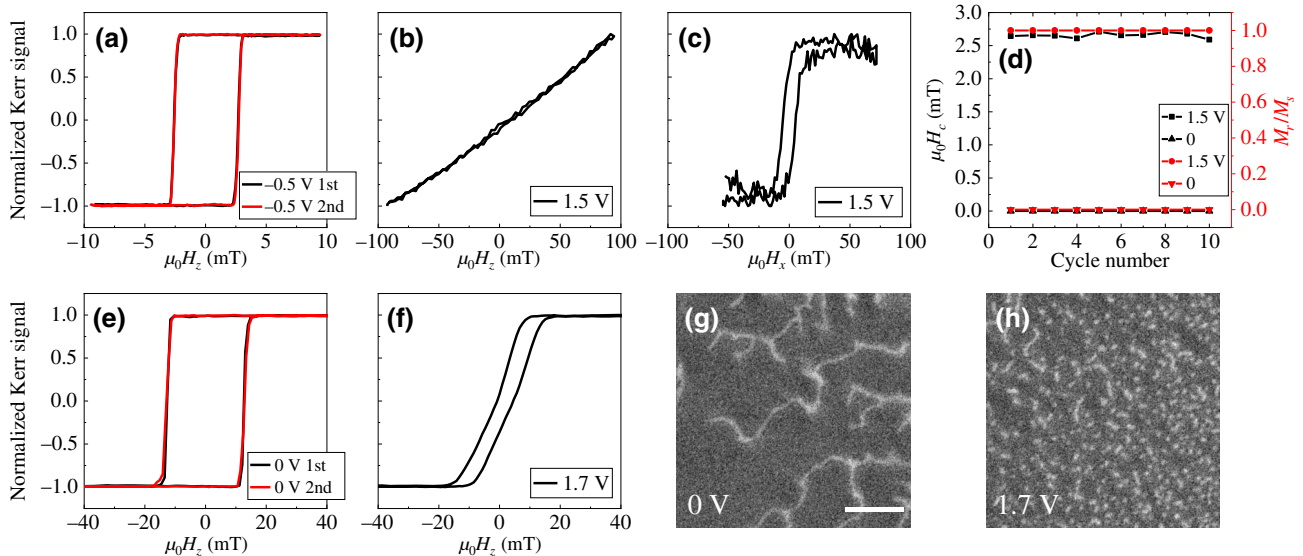

FIG. 4. The volatile gating effect for hysteresis loops and magnetic domains for a MgO(1.6 nm)/Mn$_2$CoAl(2.6 nm)/Pd(3.2 nm) stack. (a),(b) Hysteresis loops measured at −0.5 and 1.5 V, respectively. (c) A longitudinal hysteresis loop as a function of the IP magnetic field at 1.5 V. (d) $\mu_0 H_c$ and M_r/M_s as a function of the cycle number at 0 and 1.5 V, respectively. (e),(f) Hysteresis loops measured at 0 and 1.7 V, respectively. (g),(h) The corresponding magnetic domain images, with $\mu_0 H_z = 1.1$ mT, captured from (e) and (f), respectively.
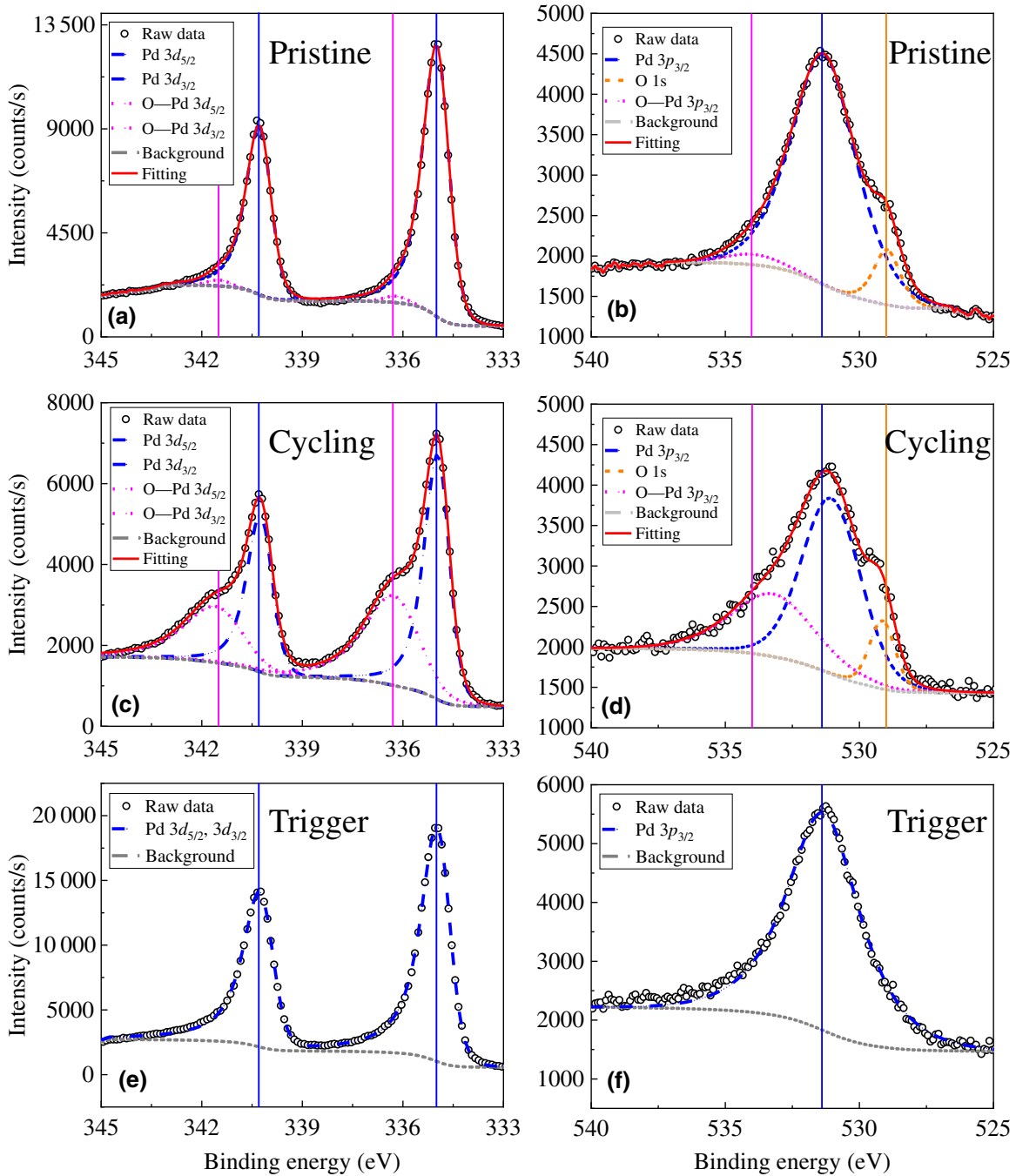
FIG. 5. The XPS spectra of trilayers at various gating conditions. The XPS spectra of (a),(b) a pristine sample [MgO(1.6 nm)/Mn$_2$CoAl(2.6 nm)/Pd(3.2 nm) stack], (c),(d) a sample [MgO(1.6 nm)/Mn$_2$CoAl(2.6 nm)/Pd(2.8 nm) stack], after cycling 31 times to the skyrmion region, and (e),(f) a sample [for MgO(1.6 nm)/Mn$_2$CoAl(2.6 nm)/Pd(3.2 nm) stack], after giving a trigger -3 V.

here from originating in either of these layers. The mean escape depth of O 1s is smaller than 2.42 nm [34], while both MgO and SiO$_2$ are covered by 2.6-nm Mn$_2$CoAl and 2.8–3.2-nm Pd layers. It should be also noted that for both stacks, with either a 2.8-nm or a 3.2-nm Pd layer thickness, the XPS results of the samples in the pristine state are the same. Therefore, all samples show the same initial condition before gating. A fresh sample is used before

carrying out processes (i), (ii), and (iii), respectively, as mentioned in Sec. II. For the intermediate-PMA sample with a 2.8-nm Pd layer, after cycling the gate voltage from -2.5 to 1 V 31 times, as shown in Fig. 3, there are obviously broad peaks of O—Pd bonds appearing at the same binding energy as they do in the pristine sample, as shown in Figs. 5(c) and 5(d). Also, the peak of the O 1s spectrum can now be clearly observed. However, for the weak-PMA

sample with a 3.2-nm Pd layer after applying a trigger voltage of -3 V (see Fig. 4), only pure Pd $3d$ and $3p$ peaks are observed, as shown in Figs. 5(e) and 5(f), which suggests that the native-oxide PdO_x layer is no longer present.

IV. DISCUSSION

Here, referring to the XPS measurements, we discuss the mechanisms that result in the nonvolatile and volatile skyrmion generation by ILG at different charge methods. There are three potential mechanisms: electrostatic charging, the magneto-ionic effect, and electrochemical reaction. The electrostatic charging is due to charge accumulated at the surface that generates a volatile ultrahigh electric field, which could change the charge-carrier density [20] and the interfacial spin-orbit coupling of thin films [21]. The magneto-ionic effect and the electrochemical reaction are due to the ion-diffusion [35] and redox reactions [36], respectively, which are expected to induce a nonvolatile effect.

It is known that there is a considerable amount of residual water (approximately 391 p.p.m. by mass) in the hydrophobic ionic liquid DEME TFSI [37]. In this situation, the O^{2-} or H^+ ions can be driven into thin films by ILG with a bias voltage due to the H_2O hydrolysis in the ambient atmosphere above 1.23 V [38] and therefore the phase [37,39] and the magnetic anisotropy [40] can be changed. For the weak-PMA thin film after applying a negative gate voltage, the O^{2-} ions from the hydrolyzed water are driven toward the Pd layer and form a slightly thicker PdO_x layer, inducing the reduction of $\mu_0 H_c$. At -2.5 V, both the PMA and the DMI decrease to a critical value at which skyrmions can be formed. On the other hand, by applying a comparatively small positive voltage where part of the O^{2-} ions can be pumped out, the value of $\mu_0 H_c$ can be partially reversed.

For the sample with intermediate PMA with a 2.8-nm Pd layer by the cycling gate voltage, the evolution of $\mu_0 H_c$ can be explained by the oxidized Pd layer if we suppose that the thicker the oxidized PdO_x layer is, the smaller is $\mu_0 H_c$. After the first couple of -2.5-V cycles, $\mu_0 H_c$ decreases rapidly as the O^{2-} ions easily diffuse into the Pd layer [see Fig. 3(i)]. After more cycles, $\mu_0 H_c$ decreases more slowly and tends toward saturation, which suggests that it becomes harder for the O^{2-} ions to diffuse deeper into the Pd and, finally, it stabilizes at -2.5 V after cycling 30 times. Here, after applying 1 V, $\mu_0 H_c$ could partially reverse, which means that there are still residual O^{2-} ions that cannot be removed from the Pd layer. Essentially, for our first two ILG methods, where the maximum gate voltage applied is -2.5 V, the mechanism is the magneto-ionic effect, because the O^{2-} ions diffuse into the surface and oxidize the Pd layer, which reduces K_{eff} and the DMI and thus generates skyrmions in a nonvolatile mode. It should be noted that the O^{2-} ions only diffuse into the Pd layer and

do not reach the Mn_2CoAl layer. This has been confirmed by the XPS depth profile (see the Supplemental Material [26]). Furthermore, the electrochemical reaction effect can be ruled out because the hysteresis loops are unchanged after charging for 5, 28, and 44 min at -2.5 V, respectively (see Fig. S3 in the Supplemental Material [26]).

For the sample after applying a trigger voltage of -3 V, the lack of a O—Pd bond in XPS, as shown in Figs. 5(e) and 5(f), indicates that the native-oxide PdO_x layer in the pristine state is etched away as we reach the edge of the electrochemical potential window of DEME TFSI (-3 to 2.7 V) [41]. Thus, the ionic liquid is in direct contact with the pure Pd layer, which could induce a significantly large electrostatic charge effect without PdO_x shielding. With an external electric field, Zhao *et al.*, have found that the distribution of the charge density in a heavy metal can be varied, resulting in a changing of the spin-orbit coupling energy and a Rashba effect in a Au/DEME TFSI/Pt/$(Co/Pt)_2$/Ta capacitor heterostructure with PMA [21]. For the Rashba effect, the spin degeneracy is removed under an electric field due to the spin-orbit interaction and leads to an effective magnetic field [42]. As our films have a similar ferromagnetic–heavy-metal structure to the PMA films of Ref. [21], this suggests that the volatile electrostatic changes in anisotropy and in the DMI in our films subjected to the trigger voltage have the same origin, namely a Rashba field induced by the gate voltage. In Ref. [21], the Rashba field causes the easy axis to change from the OP to the IP direction in a volatile mode at a positive gate voltage, exactly as we have found. By carefully decreasing the magnetic anisotropy, closing to the spin-reorientation transition, the skyrmions can be formed in a volatile state. The strength of the DMI and the Rashba field are both related to the spin-orbit coupling at the ferromagnetic–heavy-metal interface. The electric field produced by a gate voltage changes the distribution of the charge density, which in turn changes the spin-orbit coupling. Recently, an experiment [43] has demonstrated that a sufficient DMI can be induced by the Rashba effect, which could be a contribution of the volatile skyrmion in our system. Our thin films exhibit an excellent reproducibility of magnetic anisotropy to repeated gate voltages, which strongly suggests that, except for during the high-voltage trigger, no chemical reaction occurs at low voltage. Magneto-ionic gating effect has been demonstrated in Pd/Co/Pd heterostructures with PMA. In this case, H^+ ions can be pumped into the Pd layer at a positive gate voltage, which induces a $90°$ magnetization switching [40]. This gating behavior is nonvolatile and can be reversed by applying a -1 V gate voltage. In our case, the magnetic anisotropy reverses spontaneously after setting V_G back to 0 V, i.e., our gating method with a trigger produces a volatile change, which is substantially different to gating that results in a magneto-ionic effect.

V. CONCLUSION

In summary, we fabricate $MgO/Mn_2CoAl/Pd$ ultrathin films with different strengths of PMA and investigate the skyrmion generation in a nonskyrmion thickness regime by ILG. Nonvolatile skyrmions can be generated at a negative gate voltage in films with a weak PMA. For the thin films with an intermediate PMA, samples can be trained to the skyrmion regime by cycling voltages. The mechanism for both gating methods is that oxygen ions diffuse into the Pd layer and form a PdO_x layer, which induces a significant reduction of the effective magnetic anisotropy, with an extremely high anisotropy field tunability. What is more, volatile skyrmions can be created at a small positive gate voltage after applying a trigger gate voltage to etch away the native-oxide PdO_x layer. Without PdO_x shielding, an electrostatic charge accumulation happens at the surface and could induce a sufficient in-plane net Rashba magnetic field. Our results strongly demonstrate that ILG is a powerful and versatile technique toward the generation of skyrmions and skyrmion-based applications.

[1] Y. Tokura, M. Kawasaki, and N. Nagaosa, Emergent functions of quantum materials, Nat. Phys. **13,** 1056 (2017).

[2] A. Fert, N. Reyren, and V. Cros, Magnetic skyrmions: Advances in physics and potential applications, Nat. Rev. Mater. **2,** 17031 (2017).

[3] X. Zhang, Y. Zhou, K. M. Song, T.-E. Park, J. Xia, M. Ezawa, X. Liu, W. Zhao, G. Zhao, and S. Woo, Skyrmion-electronics: Writing, deleting, reading and processing magnetic skyrmions toward spintronic applications, J. Phys.: Condens. Matter **32,** 143001 (2020).

[4] X. Yu, Y. Onose, N. Kanazawa, J. Park, J. Han, Y. Matsui, N. Nagaosa, and Y. Tokura, Real-space observation of a two-dimensional skyrmion crystal, Nature **465,** 901 (2010).

[5] S. Heinze, K. Von Bergmann, M. Menzel, J. Brede, A. Kubetzka, R. Wiesendanger, G. Bihlmayer, and S. Blügel, Spontaneous atomic-scale magnetic skyrmion lattice in two dimensions, Nat. Phys. **7,** 713 (2011).

[6] S. Woo, K. Litzius, B. Krüger, M.-Y. Im, L. Caretta, K. Richter, M. Mann, A. Krone, R. M. Reeve, and M. Weigand *et al.*, Observation of room-temperature magnetic skyrmions and their current-driven dynamics in ultrathin metallic ferromagnets, Nat. Mater. **15,** 501 (2016).

[7] A. Soumyanarayanan, M. Raju, A. G. Oyarce, A. K. Tan, M.-Y. Im, A. P. Petrović, P. Ho, K. Khoo, M. Tran, and C. Gan *et al.*, Tunable room-temperature magnetic skyrmions in Ir/Fe/Co/Pt multilayers, Nat. Mater. **16,** 898 (2017).

[8] A. Bocdanov and A. Hubert, The properties of isolated magnetic vortices, Phys. Status Solidi (B) **186,** 527 (1994).

[9] I. Dzyaloshinsky, A thermodynamic theory of "weak" ferromagnetism of antiferromagnetics, J. Phys. Chem. Solids **4,** 241 (1958).

[10] T. Moriya, Anisotropic superexchange interaction and weak ferromagnetism, Phys. Rev. **120,** 91 (1960).

[11] B. Dupé, M. Hoffmann, C. Paillard, and S. Heinze, Tailoring magnetic skyrmions in ultra-thin transition metal films, Nat. Commun. **5,** 4030 (2014).

[12] M. Hervé, B. Dupé, R. Lopes, M. Böttcher, M. D. Martins, T. Balashov, L. Gerhard, J. Sinova, and W. Wulfhekel, Stabilizing spin spirals and isolated skyrmions at low magnetic field exploiting vanishing magnetic anisotropy, Nat. Commun. **9,** 1015 (2018).

[13] R. Tolley, S. Montoya, and E. Fullerton, Room-temperature observation and current control of skyrmions in Pt/Co/Os/Pt thin films, Phys. Rev. Mater. **2,** 044404 (2018).

[14] T. Srivastava, W. Lim, I. Joumard, S. Auffret, C. Baraduc, and H. Béa, Mapping different skyrmion phases in double wedges of $Ta/FeCoB/TaO_x$ trilayers, Phys. Rev. B **100,** 220401 (2019).

[15] M. Schott, A. Bernand-Mantel, L. Ranno, S. Pizzini, J. Vogel, H. Béa, C. Baraduc, S. Auffret, G. Gaudin, and D. Givord, The skyrmion switch: Turning magnetic skyrmion bubbles on and off with an electric field, Nano. Lett. **17,** 3006 (2017).

[16] T. Srivastava, M. Schott, R. Juge, V. Krizakova, M. Belmeguenai, Y. Roussigné, A. Bernand-Mantel, L. Ranno, S. Pizzini, and S.-M. Chérif *et al.*, Large-voltage tuning of Dzyaloshinskii-Moriya interactions: A route toward dynamic control of skyrmion chirality, Nano Lett. **18,** 4871 (2018).

[17] D. Bhattacharya, S. A. Razavi, H. Wu, B. Dai, K. L. Wang, and J. Atulasimha, Creation and annihilation of nonvolatile fixed magnetic skyrmions using voltage control of magnetic anisotropy, Nat. Electron. **3,** 539 (2020).

[18] C. Ma, X. Zhang, J. Xia, M. Ezawa, W. Jiang, T. Ono, S. Piramanayagam, A. Morisako, Y. Zhou, and X. Liu, Electric field-induced creation and directional motion of domain walls and skyrmion bubbles, Nano Lett. **19,** 353 (2018).

[19] C. Navarro-Senent, A. Quintana, E. Menéndez, E. Pellicer, and J. Sort, Electrolyte-gated magnetoelectric actuation: Phenomenology, materials, mechanisms, and prospective applications, APL Mater. **7,** 030701 (2019).

[20] M. Weisheit, S. Fähler, A. Marty, Y. Souche, C. Poinsignon, and D. Givord, Electric field-induced modification of magnetism in thin-film ferromagnets, Science **315,** 349 (2007).

[21] S. Zhao, L. Wang, Z. Zhou, C. Li, G. Dong, L. Zhang, B. Peng, T. Min, Z. Hu, and J. Ma *et al.*, Ionic liquid gating control of spin reorientation transition and switching of perpendicular magnetic anisotropy, Adv. Mater. **30,** 1801639 (2018).

[22] L. H. Diez, Y. Liu, D. A. Gilbert, M. Belmeguenai, J. Vogel, S. Pizzini, E. Martinez, A. Lamperti, J. Mohammedi, andA. Laborieux *et al.*, Nonvolatile Ionic Modification of the Dzyaloshinskii-Moriya Interaction, Phys. Rev. Appl. **12,** 034005 (2019).

[23] S. Z. Bisri, S. Shimizu, M. Nakano, and Y. Iwasa, Endeavor of iontronics: From fundamentals to applications of ion-controlled electronics, Adv. Mater. **29,** 1607054 (2017).

[24] B. Ludbrook, G. Dubuis, A.-H. Puichaud, B. Ruck, and S. Granville, Nucleation and annihilation of skyrmions in Mn_2CoAl observed through the topological Hall effect, Sci. Rep. **7**, 13620 (2017).

[25] Y. Zhang, G. Dubuis, T. Butler, and S. Granville, Fractal Analysis of Skyrmions Generated by Field-Assisted Fine-Tuning of Magnetic Anisotropy, Phys. Rev. Appl. **15**, 014020 (2021).

[26] See the Supplemental Material at http://link.aps.org/supplemental/10.1103/PhysRevApplied.16.014030 for details of anisotropy field fitting, the width of the domain-period calculation, the charging time effect, and the XPS depth profile. The Supplemental Material includes Refs. [25,44–48].

[27] B. Kaplan and G. Gehring, The domain structure in ultra-thin magnetic films, J. Magn. Magn. Mater. **128**, 111 (1993).

[28] Z. Qin, Y. Wang, S. Zhu, C. Jin, J. Fu, Q. Liu, and J. Cao, Stabilization and reversal of skyrmion lattice in Ta/CoFeB/MgO multilayers, ACS Appl. Mater. Interfaces **10**, 36556 (2018).

[29] G. Yu, P. Upadhyaya, X. Li, W. Li, S. K. Kim, Y. Fan, K. L. Wong, Y. Tserkovnyak, P. K. Amiri, and K. L. Wang, Room-temperature creation and spin-orbit torque manipulation of skyrmions in thin films with engineered asymmetry, Nano Lett. **16**, 1981 (2016).

[30] Y. Zhou and S. Ramanathan, Relaxation dynamics of ionic liquid–VO_2 interfaces and influence in electric double-layer transistors, J. Appl. Phys. **111**, 084508 (2012).

[31] C. Schlenker, S. Parkin, J. Scott, and K. Howard, Magnetic disorder in the exchange bias bilayered FeNi-FeMn system, J. Magn. Magn. Mater. **54**, 801 (1986).

[32] K. Kim, A. Gossmann, and N. Winograd, X-ray photoelectron spectroscopic studies of palladium oxides and the palladium-oxygen electrode, Anal. Chem. **46**, 197 (1974).

[33] W. Moddeman, W. Bowling, D. Carter, and D. Grove, XPS surface and bulk studies of heat treated palladium in the presence of hydrogen at $150°C$, Surf. Interface Anal. **11**, 317 (1988).

[34] J. Zemek, S. Hucek, A. Jablonski, and I. Tilinin, Photoelectron escape depth, J. Electron Spectros Relat. Phenomena. **76**, 443 (1995).

[35] U. Bauer, L. Yao, A. J. Tan, P. Agrawal, S. Emori, H. L. Tuller, S. Van Dijken, and G. S. Beach, Magneto-ionic control of interfacial magnetism, Nat. Mater. **14**, 174 (2015).

[36] S. Zhao, Z. Zhou, B. Peng, M. Zhu, M. Feng, Q. Yang, Y. Yan, W. Ren, Z.-G. Ye, and Y. Liu *et al.*, Quantitative determination on ionic-liquid-gating control of interfacial magnetism, Adv. Mater. **29**, 1606478 (2017).

[37] N. Lu, P. Zhang, Q. Zhang, R. Qiao, Q. He, H.-B. Li, Y. Wang, J. Guo, D. Zhang, and Z. Duan *et al.*, Electric-field control of tri-state phase transformation with a selective dual-ion switch, Nature **546**, 124 (2017).

[38] H. Ohta, Y. Sato, T. Kato, S. Kim, K. Nomura, Y. Ikuhara, and H. Hosono, Field-induced water electrolysis switches an oxide semiconductor from an insulator to a metal, Nat. Commun. **1**, 118 (2010).

[39] J. Jeong, N. Aetukuri, T. Graf, T. D. Schladt, M. G. Samant, and S. S. Parkin, Suppression of metal-insulator transition in VO_2 by electric field–induced oxygen vacancy formation, Science **339**, 1402 (2013).

[40] A. J. Tan, M. Huang, C. O. Avci, F. Büttner, M. Mann, W. Hu, C. Mazzoli, S. Wilkins, H. L. Tuller, and G. S. Beach, Magneto-ionic control of magnetism using a solid-state proton pump, Nat. Mater. **18**, 35 (2019).

[41] H. Yuan, H. Shimotani, A. Tsukazaki, A. Ohtomo, M. Kawasaki, and Y. Iwasa, High-density carrier accumulation in ZnO field-effect transistors gated by electric double layers of ionic liquids, Adv. Funct. Mater. **19**, 1046 (2009).

[42] H. C. Koo, S. B. Kim, H. Kim, T.-E. Park, J. W. Choi, K.-W. Kim, G. Go, J. H. Oh, D.-K. Lee, and E.-S. Park *et al.*, Rashba effect in functional spintronic devices, Adv. Mater. **32**, 2002117 (2020).

[43] H. Yang, G. Chen, A. A. Cotta, A. T. N'Diaye, S. A. Nikolaev, E. A. Soares, W. A. Macedo, K. Liu, A. K. Schmid, and A. Fert *et al.*, Significant Dzyaloshinskii-Moriya interaction at graphene-ferromagnet interfaces due to the Rashba effect, Nat. Mater. **17**, 605 (2018).

[44] T. Wu, H. Fu, R. Hajjar, T. Suzuki, and M. Mansuripur, Measurement of magnetic anisotropy constant for magneto-optical recording media: A comparison of several techniques, J. Appl. Phys. **73**, 1368 (1993).

[45] C. Tannous and J. Gieraltowski, The Stoner-Wohlfarth model of ferromagnetism, Eur. J. Phys. **29**, 475 (2008).

[46] P. Shepley, A. Rushforth, M. Wang, G. Burnell, and T. Moore, Modification of perpendicular magnetic anisotropy and domain wall velocity in Pt/Co/Pt by voltage-induced strain, Sci. Rep. **5**, 1 (2015).

[47] M. Yamanouchi, A. Jander, P. Dhagat, S. Ikeda, F. Matsukura, and H. Ohno, Domain structure in CoFeB thin films with perpendicular magnetic anisotropy, IEEE Magn. Lett. **2**, 3000304 (2011).

[48] N. Sato, R. M. White, and S. X. Wang, Effect of annealing on exchange stiffness of ultrathin CoFeB film with perpendicular magnetic anisotropy, Appl. Phys. Lett. **108**, 152405 (2016).